AIAA'88

AIAA-88-3265
A Navier-Stokes Study of Rotating Stall in Compressor Cascades

F. Davoudzadeh, N.-S. Liu, S.J. Shamroth and S.J. Thoren, Scientific Research Associates, Inc., Glastonbury, CT

AIAA/ASME/SAE/ASEE 24th JOINT PROPULSION CONFERENCE

July 11-13, 1988/Boston, Massachusetts

For permission to copy or republish, contact the Amerian Institute of Aeronautics and Astronautics
370 L'Enfant Promemade, S.W., Washington, D.C. 20024

A NAVIER-STOKES STUDY OF ROTATING STALL IN COMPRESSOR CASCADES

by

F. Davoudzadeh,* N.-S. Liu,** S.J. Shamroth† and S.E. Thorent††

Scientific Research Associates, Inc.

Glastonbury, CT 06033

ABSTRACT

A numerical simulation of rotating stall in a linear cascade of multiple blade passages at high Reynolds number is performed using the unsteady, two-dimensional, ensemble-averaged, compressible, time-dependent Navier-Stokes equations. The numerical scheme for solving the governing equations is the linearized block implicit algorithm which solves the equations in a coupled manner by an ADI procedure.

The propagating stall simulations were carried out for a five-passage cascade with the blading being that of a J-79 compressor stator set which had been the subject of extensive experimental investigation. A stagger angle of 40.0° and a solidity of 0.85 was chosen. The freestream Mach number was 0.4 and the Reynolds number (based upon chord length and freestream velocity) was approximately 0.6×10^5. A series of calculations were run over a range of inflow angles between 57° and 61°; at 57° inflow the angle of attack is zero. The present results indicated that these relatively small differences in inflow angle can dramatically change the flow behavior. The results of 57° inflow angle showed no stall propagation. At 60° inflow angle, the flow exhibited stall propagation under the influence of the imposed localized disturbance. However, when the disturbance was removed, the propagating cell disappeared. When the inflow angle was increased to 60.5°, this short-lived disturbance led to a rotating stall pattern which continued for three complete cycles without any significant decrease in intensity; the calculation then was discontinued. The propagation velocity was approximately 0.23 times the undisturbed upstream tangential velocity. Although certain approximations in regard to two-dimensional flow, turbulence modeling, etc., are obviously present, the results show good agreement with experimental data for rotating stall inception and show the physical features of the process.

* Research Scientist, SRA

**Senior Research Scientist, SRA; Member AIAA

† Vice President, SRA, Member AIAA

††Associate Research Scientist, SRA

Copyright © 1988 by the authors

INTRODUCTION AND BACKGROUND

The phenomena of rotating stall represents a potentially serious problem which must be recognized during the design and operation of a compression system. In rotating stall, a major separation region appears in one or more adjacent passages and this separation zone then propagates circumferentially with time. As the zone propagates to an adjacent passage, an original passage 'unstalls' and the process continues. Stall may appear as a single propagating cell or multiple propagating cells.

Rotating stall is associated with decreased compressor performance which, in itself, is a significant problem. However, the large unsteady effects associated with rotating stall can be a factor in blade fatigue and can be a precursor to destructive failure of the component. Therefore, analyses and experiments which shed further light on rotating stall phenomena represent important additions to the knowledge base.

Large scale unsteady separation is a basic feature of the process. Since rotating stall is initiated from separated flow, viscous effects which lead to and then control separation are important. Three-dimensional effects may be important; in particular, part span stall in which a stall cell occurs over only a portion of the blade passage, as well as full span stall, are both observed. Finally, in actual operation, stall may be a multi-blade row phenomena in which the presence of additional blade rows significantly affects the observed flow pattern, with the interaction effect being dependent upon blade row spacing.

Most previous efforts have approached the problem via linearized inviscid equations with the blade row represented by an actuator disc (e.g., Refs. 1-8), approaches based upon component modeling (e.g., Refs. 9-15) and approaches based upon vortex method simulation (Refs. 16 and 17).

While the works of Refs. 1-8 and other work of this type demonstrate some of the important features of rotating stall, the common approach is an inviscid one with empirical cascade turning and loss characteristics. Although inviscid flow is a reasonable assumption upstream of the blade row, it

is not downstream of the blade row where nonuniform flows associated with wakes and stall cells are important. A second drawback of this approach is the use of an empirical cascade model. It is in the blade passage region where the stall process is initiated and use of an actuator disk model here requires a specific data base. Furthermore, these approaches do not consider the basic process within the cascade and, therefore, do not give clear guidance as to how the rotating stall process may be suppressed.

The vortex method approach of Refs. 16 and 17 does not require cascade loss and turning data, but it also has limitations. As applied in Refs. 16 and 17, the flow is represented by a large collection of discrete vortices whose motions are tracked in time by an algorithm based on the two-dimensional, incompressible Euler equation. The near wall effects of viscosity are accounted for by the creation of discrete vortex sheets consistent with the no-slip condition. A semi-empirical boundary layer routine is used to estimate the locations of the separation points, and boundary vortices are released into the flow field downsteam of the separation points. It is noted here that, in many cases of practical interest, much, if not all, of the cascade passage contains viscous effects and the flow is compressible. Furthermore, it is not clear how to extend the vortex method to treat three-dimensional simulations.

The work described in the present report details the application of a two-dimensional, unsteady Navier-Stokes analysis to the rotating stall problem. Prior to discussing the work in detail, it is useful to discuss both the potential and the limitations of such an analysis. Regarding first the limitations, it is clear that a two-dimensional simulation does not contain all the relevant flow physics. A variety of experiments indicate the presence of strong radial flows when a stall cell is present; a two-dimensional analysis cannot model these three-dimensional effects. However, in many cases of practical interest, much of the flow is essentially two-dimensional. In the early stages of rotating stall, or for conditions at which rotating stall first occurs, the propagating stall zone is expected to be relatively weak and the flow is expected to remain essentially two-dimensional. Therefore, a two-dimensional approach to the early stages of this process or to conditions at which this process first occurs, i.e., incipient rotating, is a reasonable one. A second major limitation of a Navier-Stokes procedure is that of turbulence modeling. Appropriate turbulence modeling for highly three-dimensional, unsteady flows, such as those found in a fully developed rotating stall cell, is still a significant problem. However, as in the case of the two-dimensional limitation, the turbulence model is not a major problem for calculation during the inception period. A final limitation is that of computer run time. In this regard, significant progress has been made over the last few years in hardware, software and algorithm technology and cost per calculation is expected to continue to decrease.

In regard to the benefits of the present approach, the present approach considers a simulation based upon solution of the Navier-Stokes equations. When combined with a suitable turbulence model, these equations represent the actual flow physics. Although two-dimensional and turbulence model assumptions, along with grid resolution questions, still must be addressed, the present Navier-Stokes approach represents an initiation of a basic study of this very complex problem. It can include inlet distortion and large amplitude disturbance effects and has the potential for extension to three dimensions. Whereas actuator disk type approaches (e.g., Refs. 1-8) require cascade turning and loss correlations as a function of flow conditions, the present approach models these properties via a solution of the governing partial differential equations. In this manner, the present Navier-Stokes approach has the potential for assessing the effect of geometric and flow condition details.

The work presented herein represents a first application of the Navier-Stokes equations to the rotating stall problem. Details of the equations, analysis, numerical method, grid and results are given in the following sections.

Governing Equations

The equations used are the ensemble-averaged, time-dependent Navier-Stokes equations which can be written in vector form as

Continuity

$$\frac{\partial \rho}{\partial t} + \nabla \cdot \rho \vec{U} = 0 \qquad (1)$$

Momentum

$$\frac{\partial \rho \vec{U}}{\partial t} + \nabla \cdot (\rho \vec{U}\vec{U}) = -\nabla P + \nabla \cdot (\overleftrightarrow{\pi} + \overleftrightarrow{\pi}^T) \qquad (2)$$

Energy

$$\frac{\partial \rho h}{\partial t} + \nabla \cdot (\rho \vec{U} h) = -\nabla \cdot (\vec{Q} + \vec{Q}^T) + \frac{DP}{Dt} + \phi + \rho\varepsilon \qquad (3)$$

where ρ is density, $\vec{U}$ is velocity, P is pressure, $\overset{\leftrightarrow}{\pi}$ is the molecular stress tensor, $\overset{\leftrightarrow}{\pi}^T$ is the turbulent stress tensor, h is enthalpy, $\vec{Q}$ is the mean heat flux vector, $\vec{Q}^T$ is the turbulent heat flux vector, Φ is the mean flow dissipation rate and ε is the turbulence energy dissipation rate. If the flow is assumed as having a constant total temperature, the energy equation is replaced by

$$T_t = T + \frac{q^2}{2C_p} = \text{constant} \qquad (4)$$

where T_t is the stagnation temperature, q is the magnitude of the velocity and C_p is the specific heat at constant pressure. In most cases considered in this work, the total temperature has been assumed constant. This assumption was made to reduce computer run time when the constant T_t assumption was warranted.

Numerical Method

In regard to the numerical method, the basic method used is that of Briley and McDonald (Refs. 18-19) which is a Linearized Block Implicit ADI procedure. The method can be outlined as follows: the governing equations are replaced by an implicit time difference approximation, optionally a backward difference or Crank-Nicolson scheme. Terms involving nonlinearities at the implicit time level are linearized by Taylor series expansion about the solution at the known time level, and spatial difference approximations are introduced. The result is a system of multidimensional coupled (but linear) difference equations for the dependent variables at the unknown or implicit time level. To solve these difference equations, the Douglas-Gunn procedure for generating alternating-direction implicit (ADI) splitting schemes as perturbations of fundamental implicit difference schemes is introduced in its natural extension to systems of partial differential equations. This ADI splitting technique leads to systems of coupled linear difference equations having narrow block-banded matrix structures which can be solved efficiently by standard block-elimination methods.

The method centers around the use of a formal linearization technique adapted for the integration of initial-value problems. The linearization technique, which requires an implicit solution procedure, permits the solution of coupled nonlinear equations in one space dimension (to the requisite degree of accuracy) by a one-step noniterative scheme. Since no iteration is required to compute the solution for a single time step, and since only moderate effort is required for solution of the implicit difference equations, the method is computationally efficient; this efficiency is retained for multidimensional problems by using ADI matrix splitting techniques. The method is also economical in terms of computer storage, in its present form requiring only two time levels of storage for each dependent variable. Furthermore, the splitting technique reduces multi-dimensional problems to sequences of calculations which are one-dimensional in the sense that easily-solved narrow block-banded matrices associated with one-dimensional rows of grid points are produced. Consequently, only these one-dimensional problems require rapid access storage at any given stage of the solution procedure, and the remaining flow variables can be saved on auxiliary storage devices if desired. Since each one-dimensional split of the matrix produces a consistent approximation to the original system of partial differential equations, the scheme is termed a consistently split linearized block implicit scheme. Further details of the procedure are given in Refs. 18-19.

Boundary Conditions

Boundary conditions play a major role in obtaining accurate solutions and rapid numerical convergence. The boundary conditions used are based upon the suggestion of Briley and McDonald (Ref. 20). For situations having a subsonic inflow such as those considered in the current effort, total pressure, total temperature and flow angle are specified on the upstream boundary as boundary conditions. Since a fourth numerical condition is required, the second derivative of pressure is usually set to zero. For subsonic outflow conditions, static pressure is set as a boundary condition and second derivatives of temperature and velocity components are set to zero. The periodic boundaries are treated implicitly, i.e., the values of corresponding grid points on the boundaries are set to be equal during the solution process. At solid boundaries, i.e., the blade surface, no slip conditions are enforced and the blade wall temperature is specified. It should be noted that the present approach utilizes very high grid resolution near the blade surface to allow adequate specification of this important region. In general, at least one grid point falls within the viscous sublayer, $y^+<10$. This allows rigorous specification of no slip conditions without resorting to wall function formulations. Although wall function formulations may be viable in some cases, such as attached, two-dimensional flow, their application to three-dimensional, unsteady and/or separated flows is much more questionable. As a final wall condition, the normal pressure gradient is set to zero. Both the upstream and downstream boundaries have boundary conditions associated with them which are nonlinear functions of the dependent variables. These are specification of total pressure on the upstream boundary and static pressure on the downstream

boundary. These nonlinear boundary conditions are linearized in the same manner as the governing equations (via a Taylor expansion of the dependent variables in time), and then solved implicitly along with the interior point equations.

Turbulence Models

As discussed in the Background section, turbulence modeling for complex flows still remains an important issue. In the present effort a simple mixing length model was used. The model was divided into wall and wake regions. In both regions the turbulent viscosity was related to the mean flow field via

$$\mu_T = \rho \ell^2 \left(\left(\frac{\partial u_i}{\partial x_j} + \frac{\partial u_j}{\partial x_i} \right) \frac{\partial u_i}{\partial x_j} \right)^{1/2} \qquad (5)$$

where μ_T is the turbulent viscosity, ρ is the density, ℓ is the mixing length, u_i is the i^{th} velocity component and x_i is the i^{th} Cartesian direction. Summation is implied for the repeated indices. The question now arises as to specification of ℓ. For the region upstream of the trailing edge, the mixing length is specified in the usual boundary layer manner; i.e.,

$$\ell = \kappa z (1 - e^{-z^+/27}) \quad \ell \leq \ell_{max} \qquad (6)$$

where κ is the von Karman constant and z^+ is the dimensionless normal coordinate, $z u_\tau / \nu$. In boundary layer analysis, ℓ_{max} is usually taken as 0.09δ where δ is the boundary layer thickness taken as the location where $u/u_e = 0.99$. However, this definition of δ assumes the existence of an outer flow where the velocity u_e is independent of distance from the wall at a given streamwise station, i.e., it assumes u_e is only a function of the streamwise coordinate. Although a boundary layer calculation will yield solutions in which u approaches u_e asymptotically at distances far from the solid no-slip surface, Navier-Stokes solutions for cascade flow fields do not in general predict a region where u asymptotes to a constant value. Furthermore, measurements of the flow also show no such region to exist in general. Obviously, a proper choice of δ for the Navier-Stokes cascade analysis is not straightforward. The present formulation is based upon previous efforts which have given good results for boundary layer velocity profiles and skin friction coefficient for a variety of configurations. This formulation sets the boundary layer thickness by first determining u_{max}, the maximum streamwise velocity at a given station and then setting δ via

$$\delta = 2.0 \; z_{(u/u_{max} = k_1)} \qquad (7)$$

i.e., δ was taken as twice the distance for which $u/u_{max} = k_1$ where k_1 was taken as 0.90.

The region downstream of the blade trailing edge follows the model of Rudy and Bushnell (Ref. 21). In brief, this approach calculates two mixing lengths; one of which is appropriate for the far wake and one of which is appropriate for the near wake. At each station both are calculated and the minimum of the two values used. Results shown in Ref. 21 as well as unpublished results obtained at SRA indicate this is a viable engineering approach for a variety of cases considered to date.

Numerical Dissipation

The final item to be considered is numerical or artificial dissipation. To the authors' best knowledge, all Navier-Stokes numerical analyses which are applied to the high Reynolds number problems typical of turbomachinery application require some artificial dissipation to suppress nonphysical spatial oscillations. Such artificial dissipation could be added via the spatial differencing formulation (e.g., one-sided difference approximations for first derivatives) or by explicitly adding an additional dissipative type term. The present authors favor the latter approach since, when an additional term is explicitly added, the physical approximation being made is usually clearer than when dissipative mechanisms are contained within numerical truncation errors, and further, explicit addition of an artificial dissipation term allows greater control over the amount of nonphysical dissipation being added. Obviously, the most desirable technique would add only enough dissipative mechanisms to suppress oscillations without deteriorating solution accuracy.

The approach used in the present effort is based upon use of a second order anisotropic artificial dissipation term. This approach has given quantitatively accurate predictions for a series of cascade and isolated airfoil calculations for surface pressure, boundary layer velocity profile, surface heat transfer, etc. (e.g., Refs. 22, 23). Details of the approach are given in Refs. 22 & 23.

Coordinate Systems

The blade considered for rotating stall simulation is that of Ludwig, Nenni and Arendt (Ref. 24) which is the stator set No. 1 from a J-79 jet engine. The blade coordinate for the midspan geometry was furnished by L. Smith and M. Suo of General Electric Company (Ref. 25). The method used for grid generation is the constructive technique described in Ref. 22. The grid used in both the single and multiple passage configuration is shown in Fig. 1. The stagger angle is 40°and solidity

is 0.85. The grid contains 149 pseudo radial lines and 35 pseudo azimuthal lines, giving a total number of 5215 grid points per passage. As can be seen, very high resolution in the pseudo radial direction is obtained in the vicinity of the blade, with the first point from the blade being approximately 0.1×10^{-3} chords from the blade. High streamwise resolution is found in the leading and trailing edge regions.

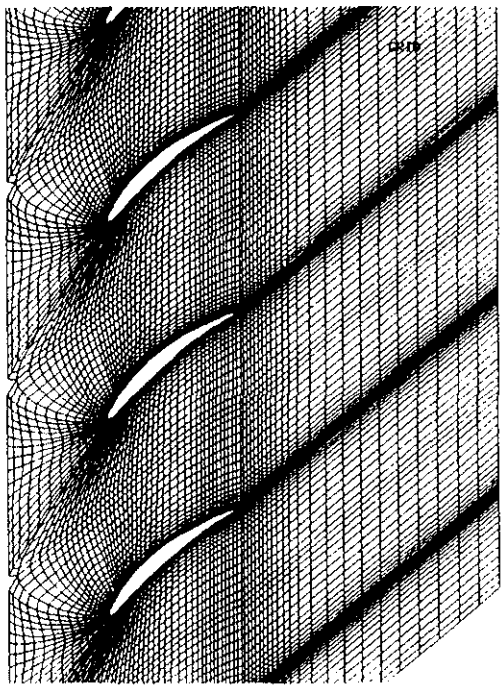

Fig. 1. Grid Distribution

NUMERICAL RESULTS

Single Passage Calculations at Different Inflow Angles

In order to qualitatively assess the performance of the numerical simulation, five different cases were carried out for a single passage flow: (1) $\alpha_1 = 57°$, (2) $\alpha_1 = 58.5°$, (3) $\alpha_1 = 59°$, (4) $\alpha_1 = 60°$, and (5) $\alpha_1 = 61°$, where α_1 is the inflow angle at the inflow boundary and $\alpha_1 = 57°$ corresponds to angle of attack of zero. The experimental relationship between α_1 and the rotating stall inception boundary is illustrated in Fig. 2, which is taken from the CALSPAN report (AFAPL-TR-73-45, Ref. 24). The parametric locations of simulated cases are also indicated in this figure. The goal of the current simulations is to assess the qualitative consistency between the experimental results and the numerical results insofar as the inception of unsteady stall is concerned. As will be demonstrated in the following results, although only a single passage was considered, the results of the numerical simulation closely follow the trend indicated by the experiments.

For cases (1)-(4), the numerical simulations all reach asymptotic steady state. The contours of axial velocity and the surface pressure distribution, for case 1 of $\alpha_1 = 57.0°$, are shown in Figs. 3-4, respectively. It should be noted that the present calculations were run at a low subsonic Mach number, $M = 0.4$, to allow transient accuracy without unrealistically limiting the allowable time step. For $M = 0.4$, the stagnation point C_p, $(P_{STAG} - P_\infty)/(1/2\rho_\infty q^2)$, should be approximately 1.045. The computed C_p is slightly above this value. As the inflow angle increases, a small recirculation region starts to develop on the suction side of the trailing edge.

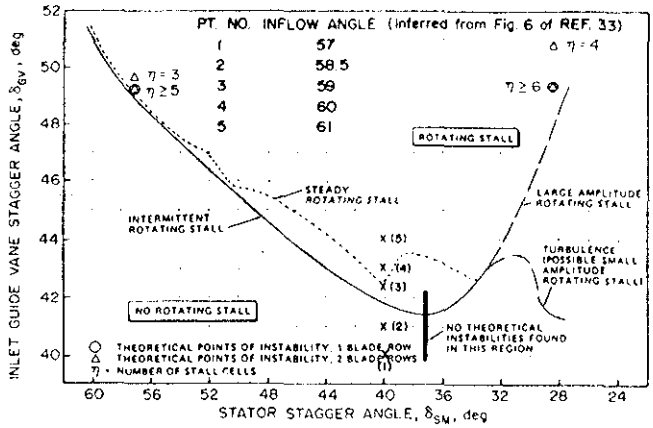

Fig. 2 Observed Rotating Stall Boundary for J-79 Stator Set No. 1 (from Ref. 24)

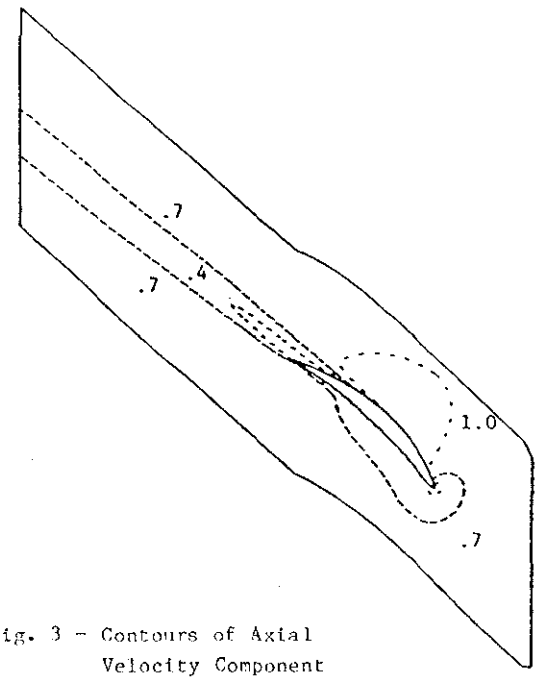

Fig. 3 - Contours of Axial Velocity Component at $\alpha_1 = 57.0°$

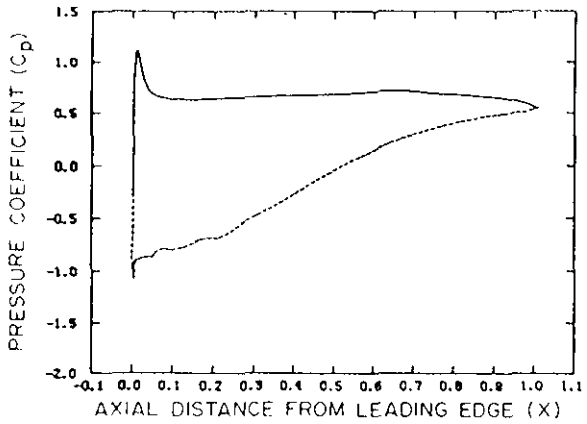

Fig. 4. Surface Pressure Distribution
$\alpha_1 = 57.0°$

The scale of the wake also increases with increasing inflow angle. Although cases (1)-(4) converge to a steady state solution, in case 5, $\alpha_1 = 61°$, the numerical simulation does not lead to an asymptotic steady state, in fact, the monitored flow quantities exhibit significant unsteadiness. A clear indication of the existence of the unsteady flow at $\alpha_1 = 61°$ is given in Fig. 5a. The recirculation region is indicated by the zero-value contour line (a solid line) in axial velocity contour plots. At $t = 0$ there is a large separation zone attached to the suction side of the trailing edge region. Subsequently, it breaks away from the trailing edge so that a relatively smaller separation region still attaches to the trailing edge while a recirculating zone of significant size appears in the near wake region as shown in Fig. 5b for $t = 14.33$. The flow situation at $t = 14.35$ is further illustrated in Fig. 6, which is a velocity-vector field. Two recirculation zones are clearly discernable. This set of simulations indicate that the inception boundary of unsteady stall for a flow with single passage periodicity, which may or may not be related to rotating stall, is approximately at $\alpha_1 = 60°$. It is of interest to note that this is the approximate inflow angle for the rotating stall boundary as given by the experimental results depicted in Fig. 2.

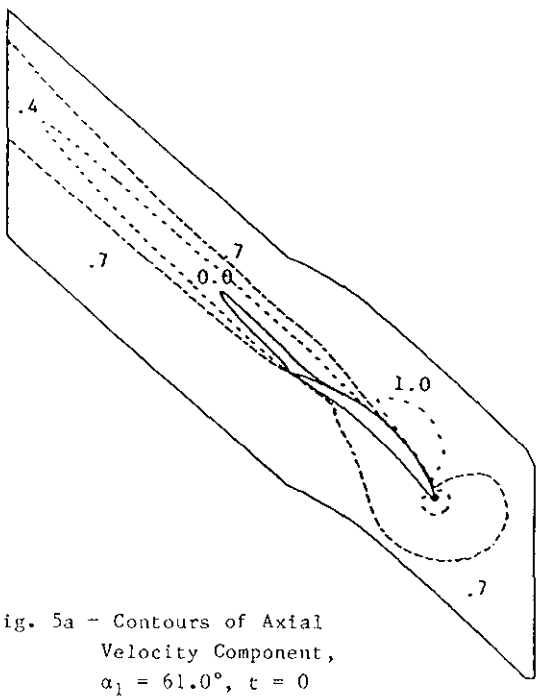

Fig. 5a – Contours of Axial Velocity Component,
$\alpha_1 = 61.0°$, $t = 0$

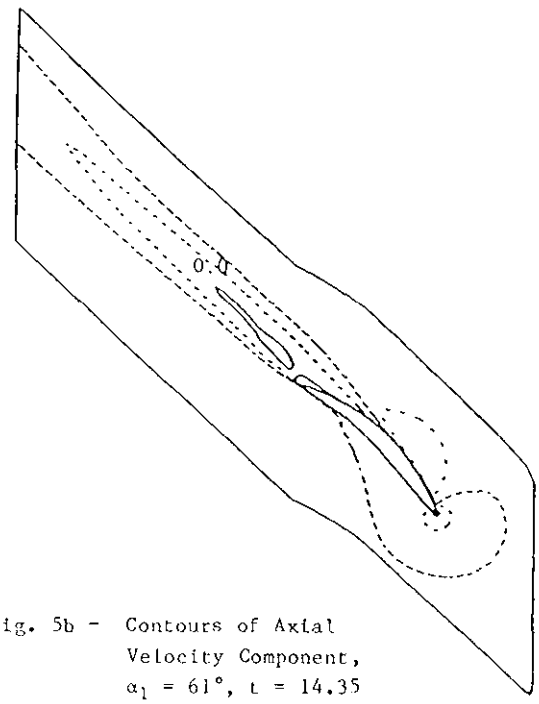

Fig. 5b – Contours of Axial Velocity Component,
$\alpha_1 = 61°$, $t = 14.35$

Single Passage Calculation with Injection

Following the single passage calculation, attention shifted to single passage calculations with wall transpiration. In initiating a rotating stall simulation, the intent is to first obtain a five passage flow in which each passage contains an identical flow field. The intent is then to introduce a disturbance, locally create a stalled passage and then follow the flow development in time. An obvious question arises in terms of how to introduce the disturbance; three obvious possibilities exist. The first possibility would introduce a disturbance in total pressure and/or flow angle at the inflow boundary. The second approach would introduce a static pressure disturbance at the outflow boundary. The final approach, which is the one used, would introduce a disturbance in the flow field. The disturbance chosen was suction surface wall transpiration over the aft 50 percent of the axial chord.

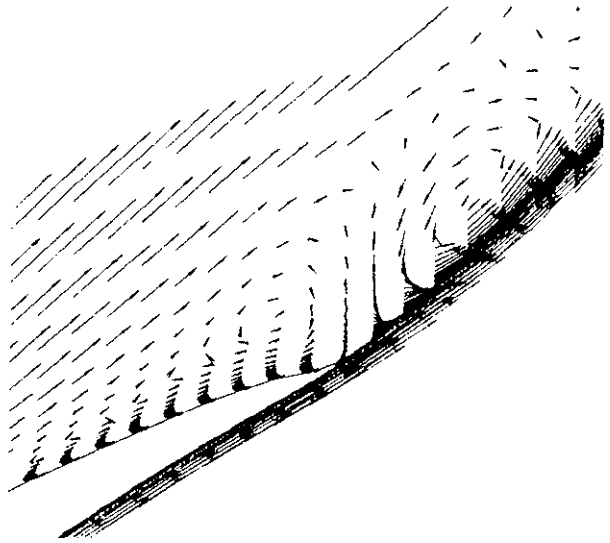

Fig. 6. Velocity Vector Field at Trailing Edge, $\alpha_1 = 61.0°$, t = 14.35

Prior to introducing the disturbance for a multiple passage calculation, the effect of a wall transpiration disturbance on a single passage flow field was considered. Two series of time accurate unsteady calculations were performed for single passage cascade flows. In the first series of calculations, the baseline flow is the steady-state solution for inflow angle of 57°. In the second series of calculations, the baseline flow is the steady-state solution for inflow angle of 60°. At some instant (i.e. t = 0), a disturbance was then applied to these baseline flows through the specification of the wall boundary condition on the suction side of the blade. More specifically, an injection toward the upstream direction was introduced (Uwall = - 0.05, Wwall = 0) in the trailing edge region. The spatial extent of the injection is about 50 percent of the axial chord length.

The first case considered is that of 57° inflow. The inclusion of a wall jet led to a change in the flow field, however, a new steady state was reached by t = 8.0. The second case considered is that of 60° inflow. In contrast to the 57° case, introduction of the wall jet led to a solution which exhibited periodic shedding and did not reach a steady state. More specifically, at t = 0.0 the disturbance was introduced into a flow exhibiting no reversed flow region; at t = 4.0, after the disturbance was in effect for 4.0 non-dimensional time units, a large separation zone developed. Subsequently, the large separation zone split into two or more separation zones proceeding downstream. At t = 24.0 the disturbance was removed, and the flow eventually returned to its initial flow field implying the uniqueness of the solution under the given inflow angle of 60.0 degrees.

Multiple Passage Calculations

The final set of calculations considered were made for a multiple passage configuration. The configuration used was a five passage linear cascade in which each passage was that of stator No. 1 of Ref. 24. This stator blade was geometrically identical to that of the fifth stage stator blade of a J-79 compressor, but with size reduced by a factor of 1.67. The tests of Ref. 24 were run at relatively low Mach number, $M_\infty \approx 0.075$. Calculations were run at a higher Mach number, $M_\infty \approx 0.4$, to avoid very small time increments which are required at lower Mach numbers due to stiffness of the equations at low Mach numbers. At $M_\infty \approx 0.4$, time increments of 0.02 were taken where a unit time increment is based upon axial chord and upstream axial velocity. In this regard, it should be noted that typical inlet Mach number conditions for actual operation are found in the high subsonic or low supersonic regime. Therefore, in practice, the restriction to moderate Mach numbers or above, if reasonable time steps are to be taken, does not represent a practical drawback. In regard to the comparison with data in the present effort, the difference in inflow Mach number condition should not be significant since the calculation was performed for flow conditions where the compressibility effects were of only moderate importance.

For multiple passage configurations, such as that shown in Fig. 1, the periodicity condition was set at both pitchwise boundaries allowing the flow to differ from passage to passage. However, if initial conditions and boundary conditions for each passage are set to be identical, an identically periodic flow field should emerge.

Calculations were run for a solidity of 0.85 and a stagger angle of 40° over a range of inflow angles. The experimental data for this configuration is shown in Fig. 2. As can be seen in this figure, at 40° stagger, no stall was observed for inflow below 58.5° and steady rotating stall was observed for inflow above 60°. In addition, at this inflow angle stall was observed to occur experimentally in a sharp and definite manner. Calculations were performed at various inflow angles by first obtaining a steady solution at that inflow angle, if such a solution existed. If a time periodic solution existed, the solution was run until a time periodic solution was obtained. In either case, a wall jet disturbance was then introduced along the suction surface of the second blade in the manner discussed in the single passage calculation. Subsequently, a stall zone appeared and if the stall zone propagated, the disturbance was removed and the evolving flow field observed. These results were then analyzed; a discussion of cases considered follows. These cases are discussed in more detail in Ref. 26.

Case No. 1 - 57°

The first case considered is that of 57° inflow. As can be seen in Fig. 2, no rotating stall should be observed under these conditions. The calculation was initiated, run to steady flow with identical flow in each passage and then a disturbance was introduced into the second passage. The disturbance consisted of wall blowing at a rate of 5 percent of the upstream velocity over the aft fifty percent of the suction surface. Within eight time units a new steady solution was obtained. However, this new flow was not periodic on a passage-by-passage basis. Furthermore, although the major disturbance was applied on the second blade, changes were also noted on both the first and third blade flow fields. Namely, a distinct and observable separation zone appeared in the aft region of the second blade suction surface, while the leading edge regions of both the first and third blades were also affected. The effective incidence on the first passage was decreased and that on the third was increased. This is consistent with the usual explanation of the rotating stall process occurring due to change in incidence of neighboring passages. According to this theory (e.g. Ref 1.), if the flow condition is such that the cascade is heavily loaded, this increase in incidence of the third passage will tend to stall the third passage. A stalled third passage then tends to relieve the second passage stall and, therefore, after some time period the stall zone originally observed on the second blade will proceed to the third blade. Although this basic mechanism of changed incidence angles was observed in this calculation, no propagation was observed under this particular inflow condition and a new steady flow pattern was attained. This is consistent with the data as shown in Fig. 2. The calculation was continued for an additional eight time units; no significant change was noted.

Case No. 2 - 61°

The second case considered was for an inflow of 61°. Again, a five passage configuration was used. With the exception of the inflow angle, conditions were identical to that of Case No. 1. As in the case of the single passage 61° calculation, a separated zone was observed. Furthermore, all passages had nearly identical flows. At t = 4.0 a disturbance in terms of a 0.02 suction surface blowing was introduced on the second blade. This was maintained until t = 8.0, when it was removed.

Table 1 presents the developing pattern between t = 12 and t = 36. As can be seen, the large separation region propagates in the direction from blade 1 to blade 5. It was clear that each passage at all times contained separated flow and although the region of most intense flow separation did propagate, passages did not fully recover. This is not usually the behavior associated with rotating stall.

	BLADE NUMBER				
t	1	2	3	4	5
12	0	0	0	X	X
16	X	0	0	X	X
20	X	X	0	0	X
24	X	X	X	0	0
28	0	0	X	X	0
32	0	0	X	X	0
36	0	0	0	X	X

Table 1 - Blade flow properties for 61° case; X indicates large separation zone; 0 indicates small separation zone.

Case No. 3 - 60°

Based upon the previous two cases, the third case was chosen at an intermediate inflow angle. Clearly, 57° inflow does not lead to any propagation, whereas 61° leads to a definite propagation. However, in this latter case no complete recovery was ever attained in any passage. Therefore, the third case was run at 60° inflow. At 60° inflow no significant separation zone existed in the absence of external disturbance. The disturbance again was introduced as a wall blowing disturbance on the suction surface of the second blade. In brief, upon introduction of the wall disturbance a significant separation zone appeared and in this case propagated toward blade 3. The wall disturbance was maintained until the separation zone reached blade 3 with some effect noted on blade 4. The upstream incidence of blades 1, 2 and 3 were affected by the blade 2 wall blowing disturbance, however, the stall propagation was limited. The disturbance was then removed and though some propagation continued, the disturbance rapidly died and the separation zone disappeared.

Case No. 4a - 60.5°

The final case considered was for an inflow of 60.5°. As will be described, three separate cases were run at this inflow angle. All cases were initiated from a solution obtained by first performing a 60.5° inflow five passage calculation and then introducing a wall blowing effect on the aft portion of the second passage. The flow pattern prior to the initiation of wall blowing is shown in Fig. 7a. As can be seen, even in the

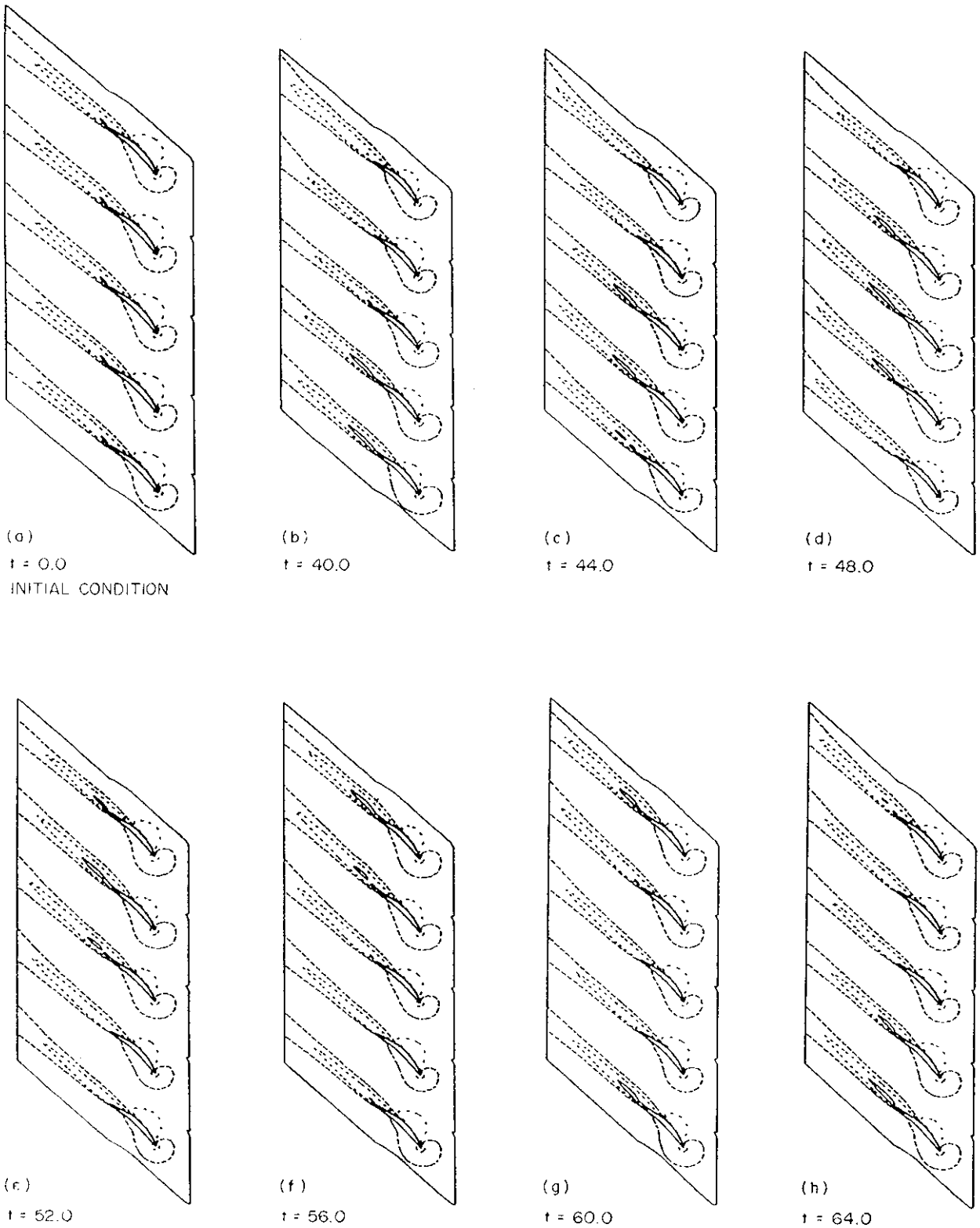

Fig. 7. - Streamwise Velocity Contours During One Complete Cycle of the Stalled Regions, 60.5° Inflow

absence of any wall blowing disturbance, a small separation region is clearly visible. In addition, the flow is essentially identical on a passage-to-passage basis. The Case 4a calculation was then initiated by introducing a disturbance in the second passage. The disturbance was held until t = 24, when it was removed. The calculation was then allowed to proceed. The time step taken in all runs was 0.02. These results showed separated flow on the first and fourth blades. As time proceeded, the pattern changed. Although the pattern did show a propagation of the separation zone(s) from passage to passage, the propagating pattern was in continuous change. Although the strength of the separated zone did not decrease with time as was the case for 60° inflow, an unchanging propagating pattern did not emerge. The calculation was run for nearly two cycles. Rather than continue this case, two other cases were run at the same flow conditions but with different initial disturbances. This was done to ascertain the dependence of the developed flow on the initial disturbance and in particular to try to reinforce the initial disturbance so as to obtain a single coherent propagating pattern. One of the cases, Case 4b, was continued for more than three cycles of propagation. These other two cases are now described.

Case No. 4b - 60.5°

As previously discussed, Case 4a showed development of a propagating stall region, however, an unchanging coherent pattern was not obtained. In Case 4b, the initial disturbance was reinforced at time t = 24.0, by removing the wall blowing in the second passage and introducing wall blowing in the fourth passage. The fourth passage wall blowing was maintained for 8 units of time and then was removed at t = 32.0. At t = 24.0, which was the last time step having second passage wall blowing, passages 2 through 5 showed some separation due to the passage number 2 disturbances, whereas the effect of this disturbance is to unload the first blade and have this passage flowing without separation.

At t = 32.0, which is eight time units after the jet has been removed from the second blade and imposed on the fourth blade, the separation zone was strengthened considerably and was particularly strong at the fourth passage. The disturbance then was removed; results at successive times are presented in Figs. 7b-7h which demonstrate the rotation of the stall cell through one complete cycle. The separated flow region propagate from blade to blade for approximately three complete cycles, where each cycle represents propagation through the entire pitchwise computational domain. It should be noted that at 60.5°, Case 4b conditions, the disturbance continues to propagate with undiminished strength. This clearly shows a rotating stall behavior. In addition, the pattern remained essentially identical as it propagated, in contrast to the changing propagating pattern of Case 4a.

Case No. 4c - 60.5°

The final case, Case 4c, was a continuation of the sensitivity of the resulting pattern to the initial disturbance. In this calculation the disturbance was reinforced by continuing the wall blowing on blade 2 and adding wall blowing on blades 3 and 4. The wall blowing was then removed and the resulting flow field showed a propagation disturbance field. The results were very similar to those of Case No. 4b with the same flow patterns and propagation speed, so these results will not be repeated here. The results of Case 4b and Case 4c suggest that similar rotating stall patterns could be developed from quite different initial disturbances.

SUMMARY AND CONCLUDING REMARKS

A summary of the five passage calculations is given in Table 2. The results at 57° showed that introduction of a disturbance gave significant change in the passage-to-passage flow but no propagation of the disturbance from passage to passage was noted. At 60° introduction of a disturbance again led to a loss of passage-to-passage periodicity and development of a flow separation region. Although this region did progress in the passage-to-passage direction, once the disturbance was removed, the flow returned to its original state; the propagating region generated by the disturbance was not self sustaining.

Inflow angle	Observed
57°	Steady flow with injection on. Return to original state when injection removed.
60°	Limited stall propagation with injection on. Return to original state when injection removed.
60.5°	Stall propagation with injection on. Cyclic stall propagation established after injection removed.
61°	Separation in all passages with/without injection. Propagation pattern dissimilar to that of rotating stall.

Table 2.
Summary of Five Passage Cascade Calculations

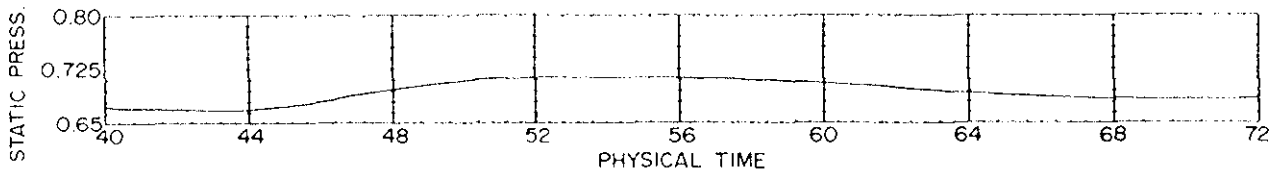

Fig. 8 - Typical Pressure Variation at the Quarter-Chord Point During the Onset-Development-Decay Cycle of the Stalled Region

The 60.5° case showed a markedly different behavior. Introduction of the disturbance led to a passage-to-passage variation and propagation of the stalled region. However, in contrast to the 60° case, propagation continued even when the disturbance was removed. Three different types of disturbance were introduced and all showed propagation; two of the three showed essentially the same flow pattern as the stall region propagated through the set of blades. One of the calculations followed the propagation over three complete cycles, during which time the disturbance showed no significant attenuation. This would associate 60.5° inflow with the inception of rotating stall for five passage periodicity. This is in good agreement with the inception noted experimentally in Fig. 2. Of course it must be noted that the present calculation assumes five passage periodicity and the effect of this assumption must be explored; nevertheless, the results give very good correspondence to the stall inception data.

In regard to the flow physics, the calculations appear to confirm the stall propagation mechanism to be a change in effective incidence due to blockage. In all of the previously discussed numerical simulations, the static pressure at the quarter-chord point on the suction side of the blade has been stored for each time step on the five blades. A comparison between these pressure-time records and the corresponding flow patterns in terms of the contours of the velocity components indicates that the blade immediately ahead of the propagating stall at first experiences an increase in the static pressure at the suction side quarter chord point. Subsequently, such an increased pressure is associated with the stall of this blade. Later, when the stall region starts to shrink, the pressure in the leading edge region also begins to decrease, until the stall region is propagated to the next blade. A typical pressure-time variation during the onset-development-decay cycle of the stalled region is illustrated in Fig. 8. Since the variation of the pressure in the leading edge region is directly related to the angle of attack, passages ahead of the propagating stall experience a reduced incidence leading to recovery from stall. Although not as clear, the increase in incidence for the passages showing trailing edge separation can also be inferred from the u and w velocity component contour plots.

Finally, as shown in Fig. 9, the decreased loading on blades having trailing edge separation is obvious from the surface pressure plots. Figure 9 compares surface pressure on blades 1 and 3 for the 60.5° inflow case correspondng to Fig. 7b. The propagation velocity appears to be approximately 0.23 times the undisturbed upstream tangential velocity. This can be interpreted as 0.23 times the wheel speed. In comparison with the results of the vortex method (Refs. 16 and 17), this propagation speed seems somewhat low. For example, the vortex method calculations of Spalart (Ref. 16) and Speziale et al. (Ref. 17) appeared to give propagation speed values of 0.38 times the wheel speed and between 0.28 and 0.47 times the wheel speed, respectively. Experimental data for stall propagation shows a wide range of results. For example, a compilation of early data given in Ref. 2 shows propagation speeds between 0.3 and 0.7 of the wheel speed with a significant dependence on disturbance wavelength, blade row geometry, flow conditions, etc. Day and Cumpsty (Ref. 27) took detailed flow measurements for stalled axial flow compressors having one to four stages. For the single stage compressors tested, the rotational speed varied between 19% and 66% of the rotational speed; obviously, the ratio of propagation speed to wheel speed does show considerable variation.

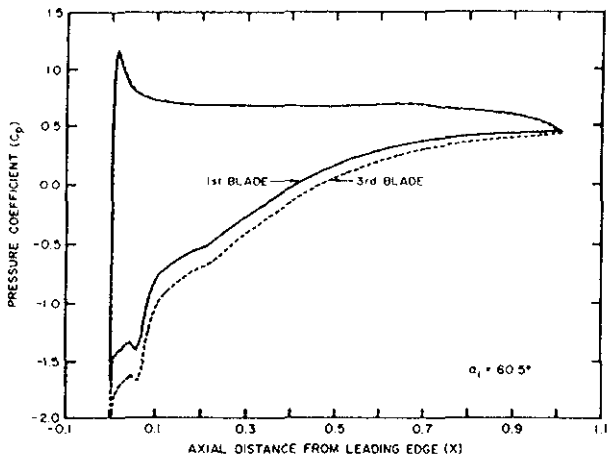

Fig. 9 - Surface Pressure Distribution on Blades Stalled (1st Blade) and Unstalled Regions (3rd Blade) of the Five Passage Cascade

The separation zones of the present simulation are significant but do not dominate the entire passage. Results showing velocity vector plots clearly delineate the separated zones and are presented in Fig. 6. The figure is from the calculation performed on a single passage cascade; for five passage cascade the separation zones were similar. In summary, although certain approximations in regard to two-dimensional flow, turbulence modeling, etc., are obviously present, the results show good agreement with data for rotating stall inception and show the physical features of the process.

ACKNOWLEDGEMENT

This work was sponsored by the Air Force Wright Aeronautical Laboratories under Contract F33615-84-C-2479. The authors gratefully acknowledge the assistance of Lt. Scott Richardson of AFWAL and Richard C. Buggeln of Scientific Research Associates during the course of this effort.

REFERENCES

1. Marble, F.E.: Propagation of Stall in a Compressor Blade Row. Journal of the Aeronautical Sciences, Vol. 22, 1955.

2. Emmons, H.W., Kronauer, R.E. and Rockett, J.A.: A Survey of Stall Propagation - Experiment and Theory. Journal of Basic Engineering, Vol. 81, 1959.

3. Takata, H. and Nagano, S.: Nonlinear Analysis of Rotating Stall. Journal of Engineering for Power, Vol. 84, 1972.

4. Adamczyk, J.J.: Unsteady Fluid Dynamic Response of an Isolated Rotor with Distorted Inflow. AIAA Paper No. 74-49, 1974.

5. Nenni, J.P. and Ludwig, G.R.: A Theory to Predict the Inception of Rotating Stall in Axial Flow Compressors. AIAA Paper 74-528, 1974.

6. Ludwig, G.D., Nenni, J.P. and Erickson, J.C., Jr.: Investigation of Rotating Stall Phenomena in Axial Flow Compressors, Vol. I - Basic Studies of Rotating Stall. AFAPL-TR-76-48, Vol. I, June 1976.

7. Ludwig, G.R. and Nenni, J.P.: Basic Studies of Rotating Stall in Axial Flow Compressors. AFAPL-TR-79-2083, September 1979.

8. Nenni, J.P., Homicz, G.F. and Ludwig, G.R.: Rotating Stall Investigations, Vol. I - Theoretical Investigations. AFWAL-TR-83-2002, 1983.

9. Greitzer, E.M.: Review - Axial Compressor Stall Phenomena. Journal of Fluids Engineering, Vol. 102, 1980.

10. Greitzer, E.M.: The Stability of Pumping Systems. Journal of Fluids Engineering, Vol. 103, 1981.

11. Cumpsty, N.A. and Greitzer, E.M.: A Simple Model for Compressor Stall Propagation. Journal of Engineering for Power, Vol. 104, 1982.

12. Moore, F.K.: A Theory of Rotating Stall of Multistage Axial Compressors: Part I - Small Disturbances. Journal of Eng. for Gas Turbines and Power, pp. 313-320, 1984.

13. Moore, F.K.: A Theory of Rotating Stall of Multistage Axial Compressors: Part V - Finite Disturbances. Journal of Eng. for Gas Turbines and Power, pp. 321-336, 1988.

14. Moore, F.K. and Greitzer, E.M.: A Theory of Post-Stall Transients in Axial Compression Systems: Part I - Development of Equations. Journal of Engineering for Gas Turbines and Power, Vol. 108, 1986.

15. Moore, F.K. and Greitzer, E.M.: A Theory of Post-Stall Transients in Axial Compression Systems: Part II - Application. Journal of Engineering for Gas Turbines and Power, Vol. 108, 1986.

16. Spalart, P.R.: Two Recent Extensions of the Vortex Method. AIAA Paper 84-0343, 1984.

17. Speziale, C.G., Sisto, F. and Jonnavithula, S.: Vortex Simulation of Propagating Stall in a Linear Cascade of Airfoils. Journal of Fluids Engineering, Vol. 108, 1986.

18. Briley, W.R. and McDonald, H.: Solution of the Multidimensional Compressible Navier-Stokes Equations by a Generalized Implicit Method, Journal of Comp. Physics, Vol. 24, pp. 372-397, August 1977.

19. Briley, W.R. and McDonald, H: On the Structure and Use of Linearized Block Implicit Schemes, Journal of Comp. Physics, Vol. 34, No. 1, pp. 54-72, January 1980.

20. Briley, W.R. and McDonald, H.: Computation of Three-Dimensional Horseshoe Vortex Flow Using the Navier-Stokes Equations, Seventh International Conference on Numerical Methods in Fluid Dynamics, Stanford University, June 1980.

21. Rudy, D.H. and Bushnell, D.M.: A Rational Approach to the Use of Prandtl's Mixing Length in Free Turbulent Shear Flow Calculations. Conferenec on Free Turbulent Shear Flows at Langley Research Center, NASA SP-321, 1973.

22. Shamroth, S.J., McDonald, H. and Briley, W.R.: Prediction of Cascade Flow Fields Using the Averaged Navier-Stokes Equations, ASME Journal of Eng. for Gas Turbines and Power, Vol. 106, No. 2, pp. 383-390, April 1984.

23. Weinberg, B.C., Yang, R.-J., McDonald, H. and Shamroth, S.J.: Calculation of Two- and Three-Dimensional Transonic Cascade Flow Fields Using the Navier-Stokes Equations, Journal of Eng. for Gas Turbines and Power, Vol. 108, pp.93-102, 1986.

24. Ludwig, G.R., Nenni, J.P. and Arendt, R.H.: Investigation of Rotating Stall in Axial Flow Compressors and Development of a Prototype Rotating Stall Control System. AFAPL-TR-73-45, 1973 (See. Also Ref. 7).

25. Smith, L. and Suo, M.: Personal Communication.

26. Davoudzadeh, F., Liu, N.S., Shamroth, S.J. and Thoren, S.J.: A Navier-Stokes study of Cascade Flow Field Including Inlet Distortion and Rotations Stall. AFWAL-TR-87-2077, 1987.

27. Day, J.J. and Cumpsty, N.A.: The Measurement and Interpretation of Flow Within Rotating Stall Cells in Axial Compressors, J. Mech. Eng. Science., Vol. 20, 1978.